GSA Data Repository item 2007114

Quantitative and qualitative insights into bedrock landform erosion on the South Indian craton using cosmogenic nuclides and apatite fission tracks, Y. Gunnell et al.; *GSA Bulletin*; May/June 2007; v. 119; no. 5/6; p. 576–585; doi: 10.1130/B25945.1

Erosion on inselberg flanks

Ramadevara Betta rises ca. 130 m above the surrounding plain. Two samples were collected for comparative purposes (cf. Fig. 6B in main manuscript): IN15 is the exposure of a curved sheet parting near the summit; and IN16 represents a residual fragment of weathered outer shell which, stratigraphically, is a downslope continuation of the layer once capping sample IN15. IN15 yields a model erosion rate (cf. Table 3 in main manuscript) of 16.7 m/m.y., much higher than neighboring IN16 (2.4 m/m.y.). However, nothing justifies such a large differential on what we believe is a slowly eroding inselberg. The simplest way to solve the paradox of such contrasting erosion rates on two adjacent bedrock surfaces is to consider that IN15 was until recently shielded at some depth below the surface, and was instantaneously exposed without giving ^{10}Be concentrations time to relax to a new steady state. In some circumstances bedrock surfaces may look natural but have been quarried, so care must be taken in distinguishing 'apparent' erosion rates (requiring correction based on observational evidence in the field) from true erosion rates. For instance, instantaneous exposure could have been caused naturally, i.e., by sheeting of the overlying slab (of which IN16 is a residual). However, IN15 occurs near the summit and critical slope angles are too low for sliding to readily occur. Instead, we suspect from the presence of a small temple nearby that stone was quarried directly from the inselberg, locally stripping the granite sheets along their natural partings. Inselberg quarrying following this technique is widely observed throughout South India. In order to test this hypothesis, we modeled the paleodepth of IN15 before its recent exposure by quarrying. Letting the surface of the sheet initially overlying IN15 erode at a similar rate to that obtained for IN16, so that the measured ^{10}Be concentration of IN15 was consistent with a steady state assumption (a condition where beryllium concentrations in the rock decrease exponentially downward from the surface), the intercept of the model curve with the measured activity level for IN15 corresponds to a paleodepth of ~1.6 m (Fig. DR1). The hypothesis that recent quarrying is responsible for the apparent offset seems valid, and we conclude that the long-term erosion rates for IN16 and IN15 are identical (ca. 2.4 m/m.y.) and therefore consistent with regional results as plotted on Fig. 7 in main the manuscript.

A neighboring bornhardt, Nijagal (Fig. 6C in main manuscript), is a dome-on-dome inselberg: it exhibits a smaller sugar-loaf hill at 1086 m a.s.l., topping a wider bedrock platform at 1050 m a.s.l., which itself stands proud of the surrounding plain by ca. 150 m. A statistically significant difference is observed between erosion rates on the apex (IN12: ca. 1 m/m.y.) and the lower rock platform (IN11 and IN13: ca. 2 m/m.y., see Table 3 in main manuscript). However, the difference is small, and the more recently exposed rock platform has most likely also reached a ^{10}Be steady state. Whatever erosion differential existed between IN12 and IN11/IN13 to generate the observed relief probably occurred earlier than the ^{10}Be detection window, and it is therefore spurious to read too much into the detected differential. Currently, all three sites are positioned in a way that makes them immune to the impacts of erosion occurring on the plain.

Fig. DR1. Model paleodepth of sample IN15 exposed by recent quarrying of overlying rock sheets.

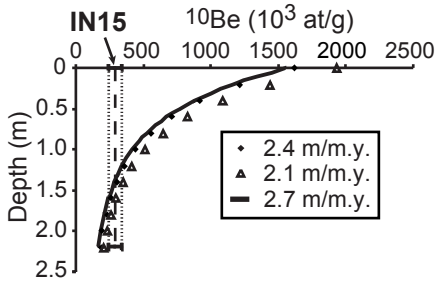

GunnellFigDR1.ai

Table DR1. AFT analytical results for the Karnataka erosional plain

Lab. No.	Latitude N			Longitude E			Elev.	Rock type	# crys-tals	Dosimetre		Spontaneous tracks		Induced tracks		Age dispersion		Central age	Mean track length	S.D.	# of confined tracks
	Deg	Min	Sec	Deg	Min	Sec	(m)			ρ_d	N_d	ρ_s	N_s	ρ_i	N_i	P(χ2)	R.E. (%)		(Ma ± 1σ)	(μm)	
IND 1835	12	22	30	75	32	00	950	charnockite	20	1.121	7769	2.570	1628	2.147	1360	15	10.0	223±10	12.10±0.20	1.95	100
IND 1845	12	56	30	76	05	40	980	gneiss	20	1.121	7769	0.877	742	0.659	557	70	0.8	248±14	12.19±0.22	2.21	100
IND 1853	12	16	45	76	40	45	1000	granite	20	1.121	7769	0.967	715	1.091	806	80	0.01	164±9	12.86±0.15	1.47	100
IND 1854	12	17	00	76	41	00	780	granite	20	1.132	7737	1.245	932	1.431	1071	30	5.1	162±8	12.78±0.17	1.78	107
IND 1859	12	53	40	75	43	50	810	gneiss	20	1.344	7449	1.514	852	1.080	608	90	0.1	312±17	11.58±0.18	1.91	108
IND 1863	12	51	20	75	51	00	930	gneiss	20	1.344	7449	1.413	1020	0.997	720	80	1.3	315±17	11.55±0.19	1.93	107
IND 1865	12	51	00	75	43	00	980	gneiss	20	1.344	7449	1.513	1101	0.929	676	90	6.8	360±19	12.61±0.19	1.99	109
IND 2052	13	40	30	75	15	00	640	gneiss	20	1.301	9015	0.738	592	0.689	553	80	0.21	232±14	11.80±0.23	2.28	100
IND 2055	13	21	55	75	32	00	750	gneiss	20	1.301	9015	1.85	1282	1.945	1348	90	0.0	206±8	12.20±0.20	2.04	104
IND 2066	14	23	00	76	05	00	660	gneiss	20	1.344	7449	1.262	953	0.998	754	30	0.92	282±14	12.17±0.20	1.97	100
IND 2067	14	16	00	76	21	00	680	gneiss	20	1.344	7449	1.494	557	1.478	551	90	0.03	226±14	11.65±0.25	2.51	100
IND 2069	13	32	00	77	00	00	780	gneiss	20	1.344	7449	1.135	1172	0.878	907	30	9.7	287±15	11.46±0.20	2.00	100
IND 2070	13	20	00	77	10	00	830	gneiss	20	1.344	7449	0.999	704	0.783	551	60	1.89	285±2	11.91±0.25	2.63	108
IND 2071	12	58	00	77	37	00	900	gneiss	20	1.344	7449	1.751	1951	1.727	1925	15	6.6	226±8	12.50±0.19	1.93	103
IND 2297	13	11	30	75	24	00	840	gneiss	20	1.364	7449	0.560	502	0.554	496	95	0.0	230±15	12.33±0.20	2.04	104
IND 2298	13	15	00	77	15	00	920	granite	20	1.364	7568	0.766	653	0.748	638	95	0.0	232±13	11.44±0.27	2.67	100
IND 2300	12	47	30	75	47	30	900	gneiss	20	1.364	7568	1.619	1048	1.165	754	40	2.2	314±16	11.89±0.19	1.92	100
IND 2305	11	24	12	76	55	13	2630	charnockite	20	1.364	7568	0.764	890	0.426	485	95	0.0	411±24	12.76±0.22	2.16	100
IND 2307	15	01	55	75	18	00	480	gneiss	20	1.364	7568	0.947	1052	0.841	935	40	7.5	255±13	11.96±0.20	2.00	102
IND 2313	13	44	00	75	00	50	600	gneiss	20	1.364	7568	1.008	953	1.067	1009	60	0.14	215±10	11.59±0.24	2.37	100
IND 2317	15	48	00	75	13	45	620	gneiss	20	1.364	7568	1.268	668	1.006	530	<1	30	291±27	12.25±0.17	1.72	101
IND 2321	15	25	25	75	26	30	630	gneiss	20	1.364	7568	0.898	561	0.835	522	<1	28.6	249±22	12.54±0.17	1.67	101
IND 2323	13	16	55	75	51	45	1000	granite	20	1.364	7568	1.635	1405	1.165	1001	30	5.4	317±14	11.27±0.18	1.81	100
IND 2325	15	33	50	75	21	00	620	gneiss	20	1.364	7568	1.771	746	1.555	655	40	9.3	258±15	11.99±0.21	2.06	102
IND 2326	13	32	00	75	20	45	760	gneiss	20	1.364	7568	0.723	608	0.626	527	80	0.3	261±16	12.13±0.24	2.45	103
IND 2327	12	02	00	77	03	00	800	gneiss	20	1.586	8792	0.492	543	0.616	681	5	17.3	217±16	12.43±0.18	1.86	102

Notes: Apatite was separated by using conventional crushing, sieving, heavy liquids, and magnetic techniques. After polishing, fluorapatite crystals > 80 μm across were etched with 5*M* HNO_3 at 20 ± 1 °C for 20 s. Low-uranium muscovite, used as an external detector, was etched with 48% HF for 50 min. Samples were irradiated at the Risø reactor (Denmark), using the Corning CN5 glass dosimeter. Analyses were carried out on a Zeiss Axioplan microscope (magnification of 1250x), using a dry (100x) objective and involving ≥100 confined track length measurements per sample.

The fission-track age is the central age, which is the mean of the log distribution of single grain ages, weighted by individual measurement precision. The 1σ error indicates the analytical precision while the standard χ^2 statistic test and the relative error were used to assess the dispersion of individual crystal ages. When P(χ^2) > 5% and R.E. < 15%, it is considered that all the apatite grains in a sample are, allowing for an acceptable level of Poissonian variation, consistent with a single population characterised by a specific fission-track age.

Quantitative thermal histories for each sample were obtained by random guided searches. This modeling procedure proposes best-estimate cooling paths based on the annealing properties of fission tracks at a range of temperatures while using a constant parameter space for temperature and time values. Here, the algorithm, recalibrated on the basis of annealing data for the widely used Durango fluorapatite age standard, was employed to predict the temperature and time dependence of annealing in the samples. Solutions are based on the statistically defined quality of match between 4000 randomly produced cooling histories per sample and the observed age and track-length data. Within the range of solutions, the highest-probability density defines an optimum, which was selected as being the most likely cooling history and hence the most probable corresponding denudation rate.